

**Syntheses and characterization of hepta-coordinated Group
4 amidinate complexes**

Journal:	<i>Dalton Transactions</i>
Manuscript ID	DT-ART-06-2018-002523.R1
Article Type:	Paper
Date Submitted by the Author:	12-Jul-2018
Complete List of Authors:	Cook, Tabitha; Berry College School of Mathematical and Natural Sciences, Department of Chemistry and Biochemistry Stere, Carlos; University of Tennessee, Department of Chemistry Xue, Zi-Ling; Univ Tennessee, Department of Chemistry

Syntheses and characterization of hepta-coordinated Group 4 amidinate complexes

Tabitha M. Cook,^{1,2} Carlos A. Steren¹ and Zi-Ling Xue^{1,*}

¹ Department of Chemistry, University of Tennessee, Knoxville, Tennessee 37996, USA

² Department of Chemistry and Biochemistry, Berry College, Mount Berry, Georgia 30149, USA

Abstract. Tri-amidinate chloride complexes $M[\text{MeC}(\text{N}^i\text{Pr})_2]_3\text{Cl}$ [$M = \text{Zr}$ (**1**), Hf (**2**)] have been prepared from MCl_4 and lithium amidinate $\text{Li}[\text{MeC}(\text{N}^i\text{Pr})_2]$. The uncommon hepta-coordinated complexes Zr-Cl (**1**) and Hf-Cl (**2**) undergo metathesis reactions with 1 equiv. of MeLi and EtMgCl to give alkyl derivatives $M[\text{MeC}(\text{N}^i\text{Pr})_2]_3\text{R}$ [$\text{R} = \text{Me}$, $M = \text{Zr}$ (**3**), Hf (**4**); $\text{R} = \text{Et}$, $M = \text{Zr}$ (**5**), Hf (**6**)]. The dynamic behaviors of Zr-Cl (**1**) and Hf-Cl (**2**) in solution have been studied using variable-temperature ^1H NMR (VT ^1H NMR), giving activation parameters ΔH^\ddagger , ΔS^\ddagger , and ΔG^\ddagger for several exchange processes in Zr-Cl (**1**) and Hf-Cl (**2**). $^1\text{H-}^{15}\text{N}$ gHMBC NMR spectroscopy gives the chemical shifts of the N atoms in **1-6**. The $^1\text{H-}^{15}\text{N}$ gHMBC NMR spectra of **1-4** at elevated temperatures are needed to obtain signals. Crystal structures of Zr-Cl (**1**), Hf-Cl (**2**), Zr-Et (**5**), and Hf-Et (**6**) have been determined via X-ray diffraction. DART-MS studies of Zr-Cl (**1**) and Hf-Cl (**2**) in air give MS of **1-2**, cations $M[\text{MeC}(\text{N}^i\text{Pr})_2]_3^+$ [$M = \text{Zr}$ (**7**), Hf (**8**)], and hydroxyl complexes $M[\text{MeC}(\text{N}^i\text{Pr})_2]_3\text{OH}$ [$M = \text{Zr}$ (**9**), Hf (**10**)]. In comparison, DART-MS spectra of **3-6** in air show only **7-8** and **9-10**, indicating lability of the alkyl ligands and/or their fast hydrolysis by the moisture.

Introduction

Many d^0 early transition metal complexes are air-sensitive and are usually handled in inert-gas environment.¹⁻²⁵ However, this sensitivity makes these complexes useful as precursors to metal oxide thin films fabricated via chemical vapor deposition (CVD) and atomic layer deposition (ALD).²⁶⁻²⁸ In these processes, late or early transition metal precursors react with oxygen sources, such as with O_2 , H_2O , or O_3 , to give metal oxide (MO_n) thin films.^{23,26,27,29-41} Amidinate ligands can bind to a wide range of metal ions, and the complexes have many applications including as catalysts or precatalysts in polymerization^{27,42,43} and hydroamination.⁴⁴ We have reported Group 4 bis-amidinate complexes and their reactivities.^{32,33,45,46} When the bis-amidinate complexes $Zr[MeC(N^iPr)_2]_2(NR_2)_2$ ($R = Me, Et$) react with O_2 , a peroxo trimer $\{(\mu-\eta^2:\eta^2-O_2)Zr[MeC(N^iPr)_2]_2\}_3$, oxo dimer $\{(\mu-O)Zr[MeC(N^iPr)_2]_2\}_2$, and polymer $\{(\mu-O)Zr[MeC(N^iPr)_2]_2\}_n$ form. Reactions of H_2O with both bis-amidinate amide complexes $Zr[MeC(N^iPr)_2]_2(NR_2)_2$ also yield $\{(\mu-O)Zr[MeC(N^iPr)_2]_2\}_2$ and $\{(\mu-O)Zr[MeC(N^iPr)_2]_2\}_n$.^{32,33}

In comparison to tetra-, penta-, and hexa-coordinated transition metal complexes, metal centers with the coordination number of seven and higher are rare because of steric and electronic restrictions.⁴⁷⁻⁵² Studies on hepta-coordinate complexes mostly pertain to their unique geometries since there is no regular polygon to adequately describe the coordination sphere.⁴⁷⁻⁵¹ Though pentagonal bipyramid is typical among the hepta-coordinate complexes, the new complexes reported herein adopt a capped octahedral geometry with three bidentate ligands and one monodentate ligand.^{53,54} Though relatively few in number, hepta-coordinated complexes are important

as, *e.g.*, intermediates in associative reactions of hexa-coordinate complexes,^{48,55} active sites of metalloproteins in biological systems,^{56,57} and polymerization catalysts.^{47,54,58}

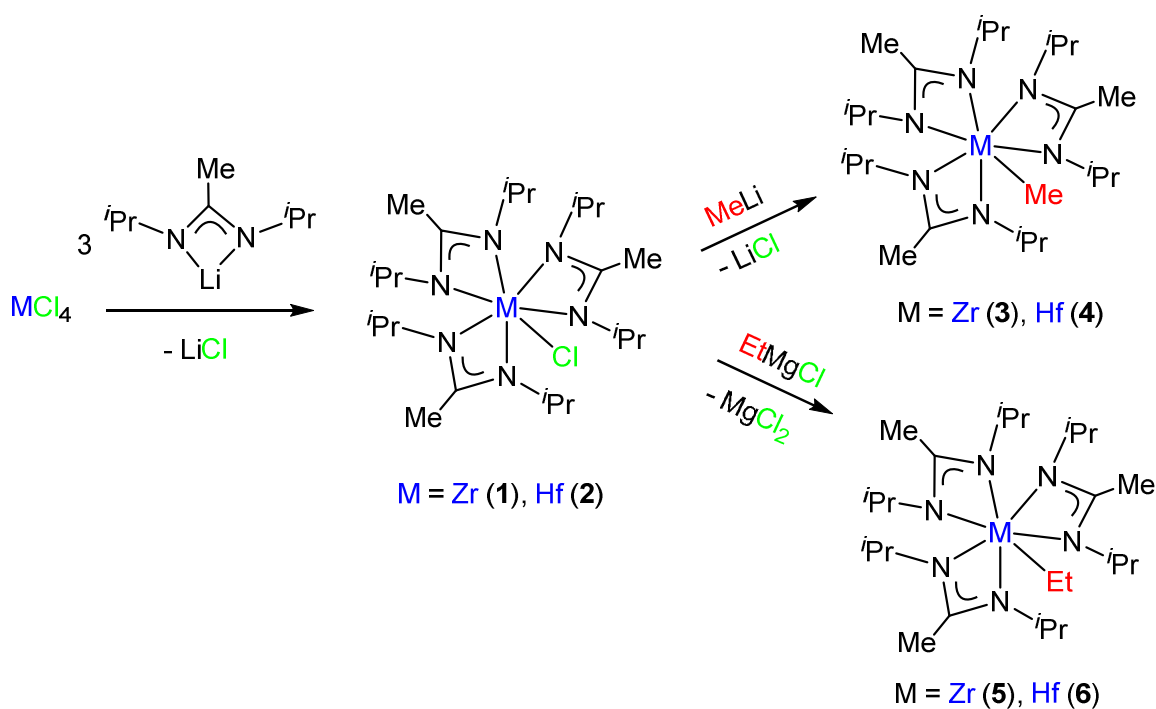
Unlike ^1H and ^{13}C NMR, ^{15}N NMR spectroscopy has not been widely used to characterize inorganic and organometallic complexes. ^{15}N NMR is difficult to acquire because it is not sensitive due to the small 0.36% natural abundance of ^{15}N and its low gyromagnetic ratio. In addition, ^{15}N NMR cannot be enhanced with techniques such as Nuclear Overhauser Effect (NOE). For d^0 complexes, there are relatively few reported ^{15}N chemical shifts. To avoid the problem of insensitivity of the nuclei, 2-D experiments such as ^1H - ^{15}N HMBC may be used. With these techniques, no enhancement is needed for the ^{15}N chemical shifts. Gómez and coworkers used ^1H - ^{15}N HMBC to obtain ^{15}N chemical shifts of several iminoacyl and imide d^0 Ta and Nb complexes.⁵⁹⁻⁶¹

In this work, we report the preparation and characterization of six d^0 hepta-coordinated Zr and Hf amidinate complexes $\text{M}[\text{MeC}(\text{N}^i\text{Pr})_2]_3\text{Cl}$ [$\text{M} = \text{Zr}$ (**1**), Hf (**2**)] and $\text{M}[\text{MeC}(\text{N}^i\text{Pr})_2]_3\text{R}$ [$\text{R} = \text{Me}$, Zr (**3**), Hf (**4**); $\text{R} = \text{Et}$, Zr (**5**), Hf (**6**)]. These complexes have been studied extensively with NMR spectroscopies, including ^1H - ^{15}N gHMBCAD. Details of the ^1H - ^{15}N gHMBCAD processes are provided. VT NMR of the chloride complexes Zr-Cl (**1**) and Hf-Cl (**2**) has been used to study the interconversion between their two enantiomers in solution. Crystal structures of Zr-Cl (**1**), Hf-Cl (**2**), Zr-Et (**5**), and Hf-Et (**6**) have been determined. Because of the bulkiness of the ligands, these complexes in solids are stable to O_2 over periods of days but react immediately with water. Though no product could be isolated, the products of the reactions of **1-6** with H_2O from air have been studied via DART-MS.

Results and discussion

Synthesis and characterizations of 1-6

$M[\text{MeC}(\text{N}^i\text{Pr})_2]_3\text{Cl}$ [$M = \text{Zr}$ (**1**), Hf (**2**)] were synthesized via salt metathesis of $\text{Li}[\text{MeC}(\text{N}^i\text{Pr})_2]$ with MCl_4 in a 2:1 hexanes:THF mixture. $M[\text{MeC}(\text{N}^i\text{Pr})_2]_3\text{R}$ [$\text{R} = \text{Me}$, Zr (**3**), Hf (**4**); $\text{R} = \text{Et}$, Zr (**5**), Hf (**6**)] were prepared by adding 1 equiv of MeLi and EtMgCl to Zr-Cl (**1**) and Hf-Cl (**2**), respectively, in Et_2O (Scheme 1). Complexes **1-6** have been studied via NMR and elemental analyses.



Scheme 1. Synthesis of **1-6**.

Zr-Cl (**1**), Hf-Cl (**2**), Zr-Et (**5**), and Hf-Et (**6**) were characterized by single-crystal X-ray diffraction. Figs. 1-2 show the ORTEPs of Hf-Cl (**2**) and Hf-Et (**6**), respectively. ORTEPs of Zr-Cl (**1**) and Zr-Et (**5**) are given in ESI (Figs. S1-S2). Zr-Cl (**1**) and Hf-Cl (**2**) adopt mono-capped octahedron geometries, and Zr-Et (**5**) and Hf-Et (**6**) assume a

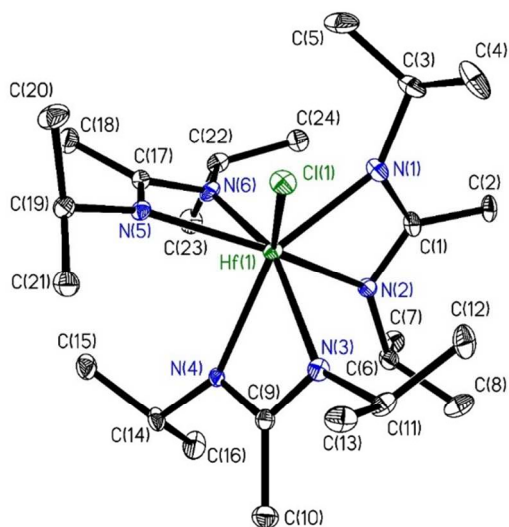


Fig. 1. ORTEP of Hf-Cl (**2**) at 100(2) K. Thermal ellipsoids are 30% probability level. H atoms were removed for clarity.

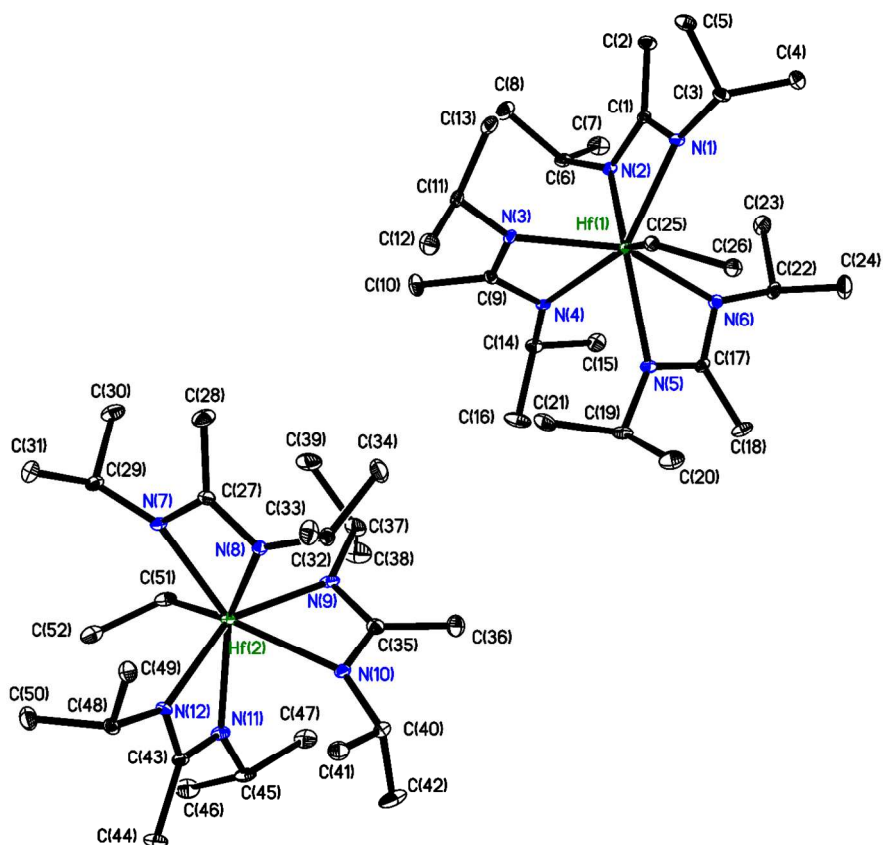


Fig. 2. ORTEP of Hf-Et (**6**) at 100(2) K showing two slightly different molecules of Hf-Et (**6**). Thermal ellipsoids are 30% probability level. H atoms were removed for clarity.

pseudo-capped octahedron geometries.^{47,50} The Δ and Λ enantiomers are both present in the unit cells.

The Zr(1)-Cl(1) bond in **1** (2.5125 Å) is longer than those in Zr[NMeC(*i*Pr)₂]₂Cl₂, which has an average length of 2.430 Å, reported by Xie and coworkers.⁴⁶ However, the Zr-Cl bond length in **1** is similar to that (2.512 Å) in the hepta-coordinated guanidinate compound [PhNC(NMe₂)NSiMe₃]₃ZrCl.^{46,58} The Hf(1)-Cl(1) bond length in **2** is 2.5014 Å, shorter than the Zr(1)-Cl(1) bond but longer than those (2.422 and 2.413 Å) in Hf[NMeC(*i*Pr)₂]₂Cl₂ reported by Devi and coworkers.⁶² The unit cells of Zr-Et (**5**) and Hf-Et (**6**) each contain two unique molecules. These molecules differ slightly on the dihedral angles between the propellers, or the plane created by the metal center and the two N atoms on the same amidinate ligand. The average length of the Hf-C bonds is 2.296 Å, which is shorter than the average length of the Zr-C bonds in **5** (2.318 Å), but longer than the Hf-C bond in Hf[MeC(*i*Pr)₂]₂Me₂.⁶² The average M-N bond lengths in Zr-Et (**5**) (2.282 Å) and Hf-Et (**6**) (2.265 Å) are slightly larger than those in their chloride analogues Zr-Cl (**1**) (2.258 Å) and Hf-Cl (**2**) (2.240 Å), respectively. The longer M-Cl, M-C, and M-N bonds in the hepta-coordinated complexes than those in hexa-coordinate complexes may be attributed to the presence of the extra ligand in the former.

Zr-Cl (**1**), Hf-Cl (**2**), Zr-Et (**5**), and Hf-Et (**6**) all have an average NCN bond angle of 112°, which is comparable to the average of the reported amidinate complexes, such as Zr[NMeC(*i*Pr)₂]₂Cl₂ (112°),⁴⁶ $\{(\mu\text{-}\eta^2\text{:}\eta^2\text{-O}_2)\text{Zr}[\text{MeC}(\text{N}^i\text{Pr})_2]_2\}_3$ (113°),³² and Zr[CyNC(Me)NCy]₂(NMe₂)₂ (113°).⁴⁵ The average bite angles of the amidinate ligands in Zr-Cl (**1**) and Hf-Cl (**2**) are 58.6° and 59.1°, respectively. These are smaller than those

in Zr[NMeC(*i*Pr)₂]₂Cl₂⁴⁶ (60.2°) and Hf[NMeC(*i*Pr)₂]₂Cl₂ (61.0°).⁶² In other words, likely due to steric effects, the bite angles of the amidinate ligands in the hepta-coordinate Zr-Cl (**1**) and Hf-Cl (**2**) are smaller than those of the hexa-coordinate analogues. The bite angles in **1-2** are similar to those in bulky amidinate complexes, such as {(μ-η²:η²-O₂)Zr[MeC(N*i*Pr)₂]₂]₃ (58.5°)³² and Zr[(CyN)₂CMe][(CyN)₂CNMe₂](NMe₂)₂ (58.6°).⁶³ The average bite angles in the amidinate ligands of Zr-Et (**5**, 58.6°) and Hf-Et (**6**, 58.4°) are smaller than their chloride analogues Zr-Cl (**1**) and Hf-Cl (**2**) probably because the ethyl ligand is bulkier than the Cl ligand.

Zr-Cl (**1**) and Hf-Cl (**2**) were also characterized directly by DART-MS (Direct Analysis in Real Time-Mass Spectrometry) with *m/z* = 549.33848 and 639.35548 (peaks of highest abundance) for [**1**+H⁺] and [**2**+H⁺], respectively. Zirconium and hafnium have five (⁹⁰Zr, ⁹¹Zr, ⁹²Zr, ⁹⁴Zr, and ⁹⁶Zr) and six (¹⁷⁴Hf, ¹⁷⁶Hf, ¹⁷⁷Hf, ¹⁷⁸Hf, ¹⁷⁹Hf, and ¹⁸⁰Hf) stable isotopes, respectively. In addition, chlorine also has two stable isotopes (³⁵Cl and ³⁷Cl). Since these isotopes have different abundances, the pattern by a monomer zirconium complex, e.g., is unique and easy to recognize and model. Calculated and observed DART-MS spectra of [**1**+H⁺] (calculated *m/z* = 549.29890) and [**2**+H⁺] (calculated *m/z* = 639.33987), as well as all other DART-MS spectra, are given in ESI (Figs. S45-S50). Since the Cl ligand is labile, the major observed species in each of the spectra are the cations, Zr[NMeC(*i*Pr)₂]₃⁺ (**7**, calculated *m/z* = 513.3222) and Hf[NMeC(*i*Pr)₂]₃⁺ (**8**, calculated *m/z* = 603.36437). Complexes **3-6** could not be directly identified by DART-MS due to lability of the alkyl ligands and/or their fast hydrolysis by the moisture. For these alkyl complexes, the cations **7-8** were again the major species present in the spectra. Complexes **1-6** also react with water from the air to form

additional species discussed below.

^1H and $^{13}\text{C}\{^1\text{H}\}$ NMR chemical shifts of **1-6** are summarized in Table 1. The ^1H signal for the CHMe_2 group in Zr-Cl (**1**) is broad (Fig. S3). However, this signal appears as a doublet for Zr-Me (**3**) (Fig. S11) and Zr-Et (**5**) (Fig. S24), with **5** showing a more resolved doublet. The features of the ^1H peaks are consistent with the need to heat the samples of Zr-Cl (**1**) at 60 °C and Zr-Me (**3**) at 45 °C in order to obtain their ^1H - ^{15}N gHMBC signals. Zr-Et (**5**) has a well-defined ^1H doublet for the CHMe_2 groups, suggesting that a fast exchange has already been achieved at 25 °C.

The ^1H NMR spectra of Hf-Cl (**2**) (Fig. S7), Hf-Me (**4**) (Fig. S16), and Hf-Et (**6**) (Fig. S30) in benzene- d_6 at 23 °C are similar to their Zr analogues with a few notable shifts in the peak positions, especially of the $\alpha\text{-C}$ and $\alpha\text{-N}$. The spectra show a multiplet for the CH moieties in the isopropyl groups in the 3.64-3.74 ppm region, a small downfield shift from the Zr analogues. Again, the CHMe_2 groups on the amidinate ligands appear differently between the three analogs. The ^1H spectrum of Hf-Cl (**2**) shows a very broad doublet. Its exchange seemed to be faster than that of Zr-Cl (**1**) and is studied in more detail below. The doublets of the CHMe_2 groups in Hf-Me (**4**) and Hf-Et (**6**) are more resolved than that of Hf-Cl (**2**). As with the Zr analog, Hf-Et (**6**) shows the most separated doublet. The chemical shift of the *Me* ligand in **4** is similar to 0.57 ppm of the Hf-*Me* peak in $\text{Hf}[\text{MeC}(\text{N}^i\text{Pr})_2]_2\text{Me}_2$ in benzene- d_6 .⁶² The *Me* peak of Hf-Me (**4**) (Fig. S17) and the peak for the CH_2 in the ethyl ligand of Hf-Et (**6**) (Fig. 31) are found to be downfield shifted from those of Zr-Me (**3**) (Fig. S12) and Zr-Et (**5**) (Fig. S25). This fits the trend that $\alpha\text{-C}$ chemical shifts of third-row elements are more downfield than their second-row congeners (*i.e.*, the first trend we reported in Ref. 64).

^1H - ^{15}N gHMBC (Gradient Heteronuclear Multiple Bond Correlation) signals are given in Table 2. The 2-D spectroscopy provides the through-bond, long-range coupling between ^1H and ^{15}N nuclei that are two or three bonds away. For **1-4**, the ^1H - ^{15}N gHMBC experiments were performed at higher temperatures in order to detect the HMBC cross peaks. This is due to slow exchanges in the complexes at room temperature. The two cross peaks for the N atoms in the ^1H - ^{15}N gHMBC spectra of Hf-Cl (**2**) (Fig. S10), Hf-Me (**4**) (Fig. S20), and Hf-Et (**6**) (Fig. S35) are also found upfield-shifted from those of Zr-Cl (**1**) (Fig. S6), Zr-Me (**3**) (Fig. S15), and Zr-Et (**5**) (Fig. S29), respectively. Since the amidinate ligand contains a resonance structure, this observation fits a second trend of the NMR chemical shifts of the α -C atoms we reported.⁶⁴ That is, a multiplet, bound α -N chemical shift is more upfield for third-row elements than for their second-row analogues.⁶⁴ Elevated temperatures (60 and 45 °C, respectively) are needed for the ^1H - ^{15}N gHMBC spectra of Zr-Cl(**1**)/Hf-Cl (**2**) and Zr-Me(**3**)/Hf-Me (**4**), while ^{15}N HMBC peaks of Zr-Et (**5**)/Hf-Et (**6**) could be readily obtained at room temperature.

Table 1. Chemical shifts in ^1H (top) and $^{13}\text{C}\{^1\text{H}\}$ (bottom) NMR spectra for **1-6** at 23 °C in benzene- d_6 .

	Chemical Shifts (ppm) from ^1H and ^{13}C spectra	Chemical Shifts (ppm) from ^1H and ^{13}C spectra
Compound	<i>Zr-Cl (1)</i>	<i>Hf-Cl (2)</i>
CHMe_2	1.33	1.33
	23.9	24.0
CHMe_2	3.53	3.65
	48.3	48.0

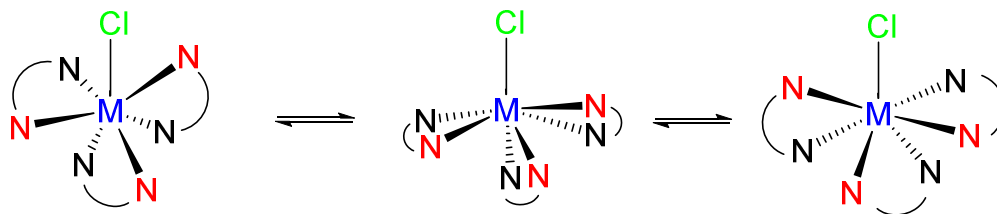
NC(Me)N	1.62	1.62
	12.8	13.3
NC(Me)N	174.7 ($^{13}\text{C}\{^1\text{H}\}$)	174.1 ($^{13}\text{C}\{^1\text{H}\}$)
	<i>Zr-Me (3)</i>	<i>Hf-Me (4)</i>
MMe	0.81	0.52
	49.4	54.7
CHMe ₂	1.28	1.27
	24.5	24.5
CHMe ₂	3.53	3.64
	48.0	47.8
NC(Me)N	1.68	1.65
	12.5	13.1
NC(Me)N	174.3 ($^{13}\text{C}\{^1\text{H}\}$)	173.4 ($^{13}\text{C}\{^1\text{H}\}$)
	<i>Zr-Et (5)</i>	<i>Hf-Et (6)</i>
CHMe ₂	1.26	1.25
	24.5	24.5
CHMe ₂	3.66	3.74
	47.6	47.4
NC(Me)N	1.71	1.69
	14.0	14.6
NC(Me)N	174.7 ($^{13}\text{C}\{^1\text{H}\}$)	173.9 ($^{13}\text{C}\{^1\text{H}\}$)
MCH ₂ CH ₃	1.85	2.01
	16.1	16.3
MCH ₂ CH ₃	1.06	0.73
	53.6	58.2

Table 2. ^{15}N chemical shifts of the ^1H - ^{15}N gHMBC NMR spectra of **1-6** in benzene- d_6 .

Compound	^{15}N shifts (ppm)	Temperature ($^{\circ}\text{C}$)
Zr-Cl (1)	-183.23, -183.09	60
Hf-Cl (2)	-188.34, -188.31	60
Zr-Me (3)	-188.78, -188.49	45
Hf-Me (4)	-191.97, -191.95	45
Zr-Et (5)	-187.95, -187.87	25
Hf-Et (6)	-191.29, -191.20	25

Dynamic behavior in ^1H NMR spectra. Comparison with the properties in ^1H - ^{15}N NMR spectra

The broad peaks in the ^1H NMR spectra for $\text{CH}(\text{Me})_2$ groups on the amidinate ligands in Zr-Cl (**1**) (Fig. S3) and Hf-Cl (**2**) (Fig. S7) suggest that they are dynamic in solution, undergoing exchanges at room temperature probably via a pseudo-Bailar twist mechanism (Scheme 2).⁶⁵ The Bailar twist mechanism occurs when two enantiomers (Δ and Λ) of an octahedral complex undergo an exchange via a trigonal prismatic intermediate. We have studied the twisting mechanism of hexa-coordinate bisamidinate bisamide complexes $\text{Zr}[\text{MeC}(\text{NR})_2]_2(\text{NMe}_2)_2$ ($\text{R} = \text{Cy}, ^i\text{Pr}$) and bisguanidinate bisamide complex $(\text{Et}_2\text{N})_2\text{Zr}[^i\text{PrNC}(\text{NEt}_2)\text{N}^i\text{Pr}]_2$.^{24,32,33,45} In the current work, VT ^1H NMR studies were conducted on Zr-Cl (**1**) (Figs. 3 and S36) and Hf-Cl (**2**) (Fig. S41). For **1**, there are two separate VT ^1H NMR studies: one at 193-313 K in toluene- d_8 (Fig. 3) and another at 280-338 K in benzene- d_6 (Fig. S36). The presence of the broad doublet in the ^1H spectrum of Zr-Cl (**1**) at room temperature suggests that the exchange between



Scheme 2. Exchange between the Δ and Λ enantiomers of Zr-Cl (**1**) and Hf-Cl (**2**).

the Δ and Λ enantiomers is faster for Hf-Cl (**2**) than for Zr-Cl (**1**). As the temperatures of these solutions are lowered, de-coalescence of the isopropyl CH and methyl groups occur. At low temperatures, rotations and exchanges are significantly slowed. ^1H NMR spectra of Zr-Cl (**1**) are taken from 193 K to 313 K (Fig. 3) in order to study the exchanges of the methyl groups and the CH moieties on the three amidinate ligands. At 193 K, the spectrum of Zr-Cl (**1**) shows four sets of doublets located at 1.64, 1.51, 1.16, and 1.13 ppm for the two sets of methyl groups Me_GMe_H and Me_EMe_F for the isopropyl groups CHMe_EMe_F and CHMe_GMe_H , respectively. As the temperature is slowly raised, the rotation rates of the methyl groups on the isopropyl groups increase until they become equivalent and reach coalescence. Since these two methyl rotations are of the same type, it is not surprising that their temperature ranges are similar at 203-238 K and 208-243 K, respectively. The next exchange observed was the pseudo-Bailar twist, which racemizes the Δ and Λ enantiomers and require higher temperatures than the simple methyl rotations discussed above. The Bailar twist is observed in the coalescences between the two isopropyl groups CHMe_GMe_H and CHMe_EMe_F (labeled as $\text{Me}_{E-F}\text{Me}_{G-H}$) as well as the H atoms (labeled as H_AH_B) of the isopropyl groups $\text{CH}_A\text{Me}_E\text{Me}_F$ (or CH_AMe_2) and $\text{CH}_B\text{Me}_E\text{Me}_F$ (or CH_BMe_2). The CH_AMe_2 and CH_BMe_2 peaks coalesce at 268(1) K, and the two sets of CHMe_2 peaks coalesce into a broad

singlet at 283(1) K, which become a doublet at 308(1) K due to the coupling to the H atoms in the CHMe_2 groups. This doublet sharpens as the temperature is increased.

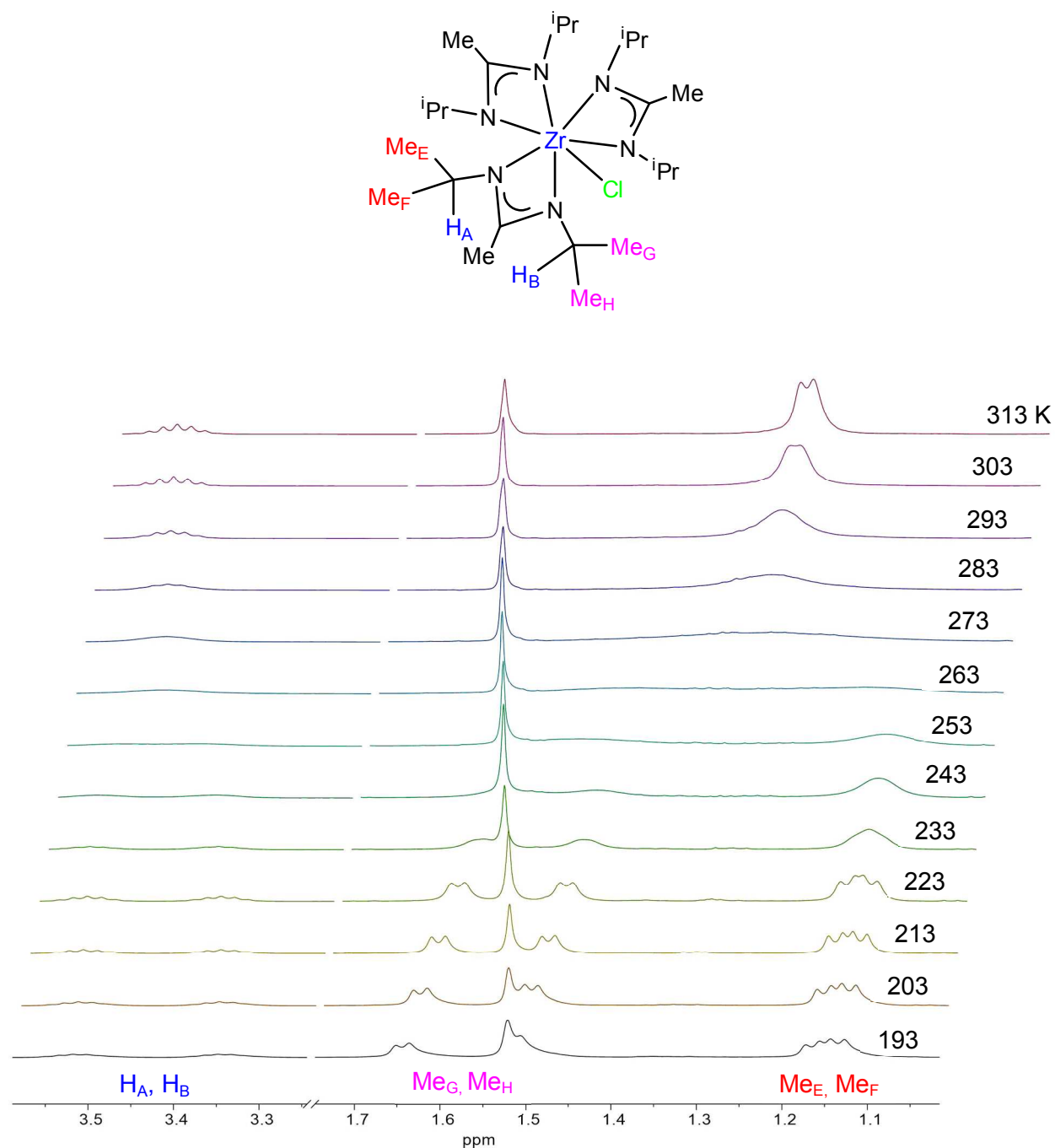


Fig. 3. Partial ^1H NMR spectra of Zr-Cl (1) in $\text{toluene-}d_8$ recorded on a 400 MHz NMR spectrometer. The CHMe_2 and CHMe_2 region is shown.

The ^1H spectra of Hf-Cl (**2**) were taken from 190 K to 300 K. The spectrum at 190 K shows four doublets at 1.64, 1.51, 1.14 and 1.12 ppm for the two sets of methyl groups in CHMe_EMe_F and CHMe_GMe_H , respectively. The doublets at 1.14 and 1.12 ppm overlap. As the temperature is raised slowly, the rates of the methyl rotations increase until these groups become equivalent and their peaks coalesce. The next exchange observed is the pseudo-Bailar twist, which is the interconversion between Δ and Λ enantiomers. This process is more difficult than the simple methyl rotations, as shown in the coalescence of the groups CHMe_GMe_H and CHMe_EMe_F (labeled as $\text{Me}_{E-F}\text{Me}_{G-H}$) at 270(1) K, which is higher than the coalescence temperatures for the methyl rotations. At 300(1) K, the CHMe_2 groups become a doublet due to the coupling to the H atoms in the CHMe_2 groups. Though the CHMe_2 multiplet is greatly broadened at 190 K and becomes a sharp multiplet as the temperature is raised, this peak never de-coalesces into CH_AMe_2 and CH_BMe_2 as that in Zr-Cl (**1**).

The kinetics of the exchanges in Zr-Cl (**1**) and Hf-Cl (**2**) have been studied. The rate constants of this interconversion at different temperatures (Tables S7 and S8) are calculated from Eq. 1.

$$k = \pi\sqrt{2(\Delta\nu_0^2 - \Delta\nu^2)} \quad (\text{Eq. 1})$$

where $\Delta\nu_0$ and $\Delta\nu$ are frequency differences (Hz) between the sites of the slow exchange limit and the exchange-broadened sites at the temperature (T), respectively.⁶⁶⁻⁶⁸

The activation parameters of the exchanges (Table 3) are determined from Eyring plots,

which are given in ESI (Figs. S37-S40, S42-S44). The frequency differences are taken from the CHMe_2 groups in Zr-Cl (**1**) and Hf-Cl (**2**) and used in Eq. 1. The Me_EMe_F and Me_GMe_H exchanges are the slow rotations of the two methyl groups on the same isopropyl groups in Zr-Cl (**1**). The methyl rotations reach coalescence first at 238(1) and 253(1) K with similar activation parameters $\Delta H^\ddagger = 4.9(3)$ and $4.1(3)$ kcal/mol and $\Delta S^\ddagger = -29(1)$ and $-31(1)$ eu for Me_EMe_F and Me_GMe_H , respectively. Both the H exchange of H_AH_B and the exchange of the two isopropyl groups $\text{Me}_{E-F}\text{Me}_{G-H}$ refer to the same pseudo-Bailar twist. Thus, their exchange temperature ranges and activation parameters are similar: $\Delta H^\ddagger = 2.6(3)$ kcal/mol and $\Delta S^\ddagger = -37(1)$ eu for the former and $\Delta H^\ddagger = 3.0(3)$ kcal/mol and $\Delta S^\ddagger = -34(1)$ eu for the latter. The values of ΔH^\ddagger and ΔS^\ddagger for the rotations of the methyl groups on the isopropyl groups (Me_EMe_F and Me_GMe_H) in Zr-Cl (**1**) as well as the exchange between them ($\text{Me}_{E-F}\text{Me}_{G-H}$) are similar to those of the methyl groups on the isopropyl groups of the guanidinate ligands in $\text{Zr}[\text{PrNC}(\text{NEt}_2)\text{N}^i\text{Pr}]_2(\text{NEt}_2)_2$.²⁴ In the hexa-coordinate $\text{Zr}[\text{PrNC}(\text{NEt}_2)\text{N}^i\text{Pr}]_2(\text{NEt}_2)_2$, rotations and exchanges are difficult as well because of the bulky guanidinate and ethyl amide ligands. The Me_EMe_F and Me_GMe_H exchanges in Hf-Cl (**2**) are the rotations of the two methyl groups on the same isopropyl groups. These methyl rotations reach coalescence first at 235(1) and 250(1) K with activation parameters $\Delta H^\ddagger = 2.84(3)$ and $4.6(4)$ kcal/mol and $\Delta S^\ddagger = -39(1)$ and $-29(1)$ eu for Me_EMe_F and Me_GMe_H , respectively. The rates of the rotations of the methyl groups as well as the rates of the interconversions between the enantiomers are slightly faster for Hf-Cl (**2**) than for Zr-Cl (**1**). The activation parameters (Table 3) for the exchanges in Zr-Cl (**1**) and Hf-Cl (**2**) show that ΔH^\ddagger is relatively small and ΔS^\ddagger is largely negative. These results reflect the

fact that no bonds are broken in the exchanges, but the bulkiness of the amidinate groups and the crowded coordination sphere make the exchanges difficult.

Table 3. Activation parameters of the interconversions in M[MeC(NⁱPr)₂]₃Cl (**1-2**).

	$H_A H_B^a$	$Me_E Me_F$	$Me_G Me_H$	$Me_{E-F} Me_{G-H}^b$
M = Zr (1)				
ΔH^\ddagger (kcal/mol)	2.6(3)	4.9(3)	4.1(3)	3.0(3)
ΔS^\ddagger (eu)	-37(1)	-29(1)	-31(1)	-34(1)
M = Hf (2)				
ΔH^\ddagger (kcal/mol)	2.84(3)	4.6(4)	3.1(3)	
ΔS^\ddagger (eu)	-39(1)	-29(1)	-33(1)	

^a H_A, H_B refers to the H atoms on the isopropyl groups.

^b Me_{E-F}, Me_{G-H} refers to the interconversion between Me_E, Me_F and Me_G, Me_H after they each have coalesced.

The Me_2CH ¹H NMR signal of Zr-Et (**5**) (Fig. S24) and Hf-Et (**6**) (Fig. S30) at 23 °C is a well resolved doublet, indicating that **5-6** are in a fast exchange. On the other hand, for the M-Cl (**1-2**) and Zr-Me (**3**) complexes, either a single broad signal or a poorly resolved doublet, is observed (See Fig. 4 for comparison of the Zr complexes) at 23 °C, suggesting that **1-3** undergo slow or intermediate exchanges. Since ¹⁵N-HMBC signals can only be observed when the molecule is in a fast exchange, the spectra of **1-4** were recorded at elevated temperatures: 45 °C for Zr-Me (**3**) and Hf-Me (**4**) and 60 °C for Zr-Cl (**1**) and Hf-Cl (**2**), as indicated earlier. The

difference in temperatures needed to obtain the coalesced ^{15}N -HMBC signals can be attributed to the length of the bonds within the complexes. The crystal structures of Zr-Cl (**1**), Hf-Cl (**2**), Zr-Et (**5**), and Hf-Et (**6**) show that the M-N bonds are, on average, longer for the ethyl compounds than the chloride compounds, as the chloride ligand is less bulky than the ethyl ligand allowing the amidinate ligands to bind more closely. Thus, the exchanges of the enantiomers are more difficult in Zr-Cl (**1**) than in Zr-Et (**5**). This same trend is observed in the Hf complexes as well. Repeated attempts to obtain crystals of either Zr-Me (**3**) or Hf-Me (**4**) for X-ray diffraction were unsuccessful. Thus, the M-N bond lengths in **3-4** cannot be determined. However, because their ^1H - ^{15}N gHMBC NMR spectra were obtained at an intermediate temperature, it may be inferred that the M-N average bond lengths in Zr-Me (**3**) and Hf-Me (**4**) are between those in Zr-Cl (**1**) or Hf-Cl (**2**) and Zr-Et (**5**) or Hf-Et (**6**), respectively.

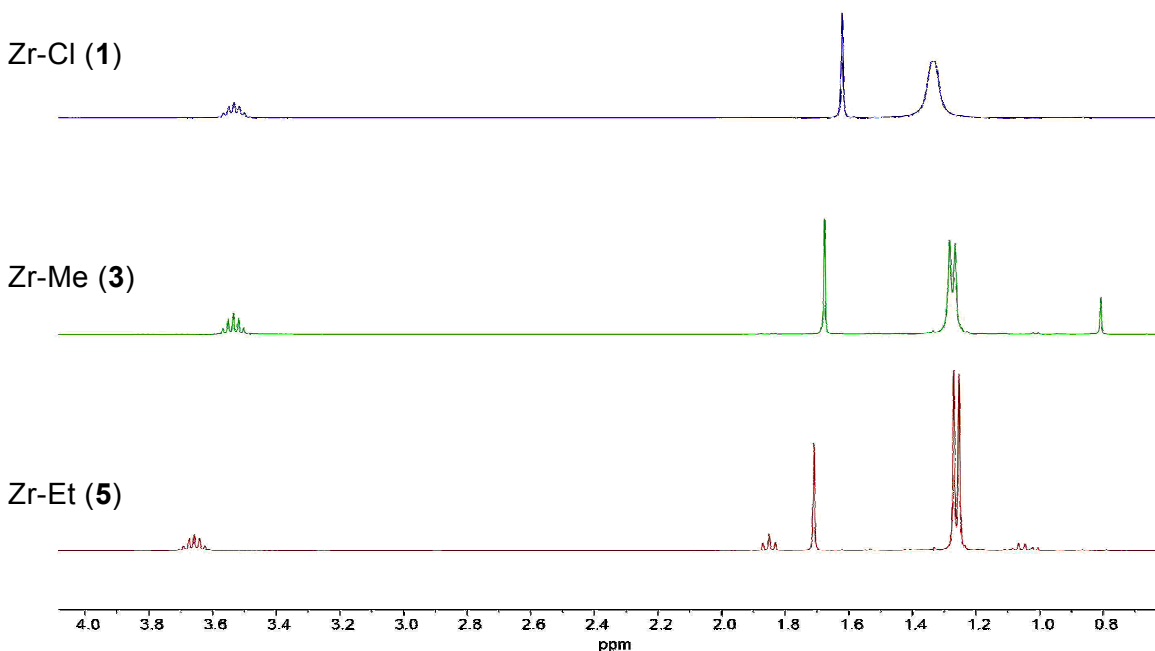


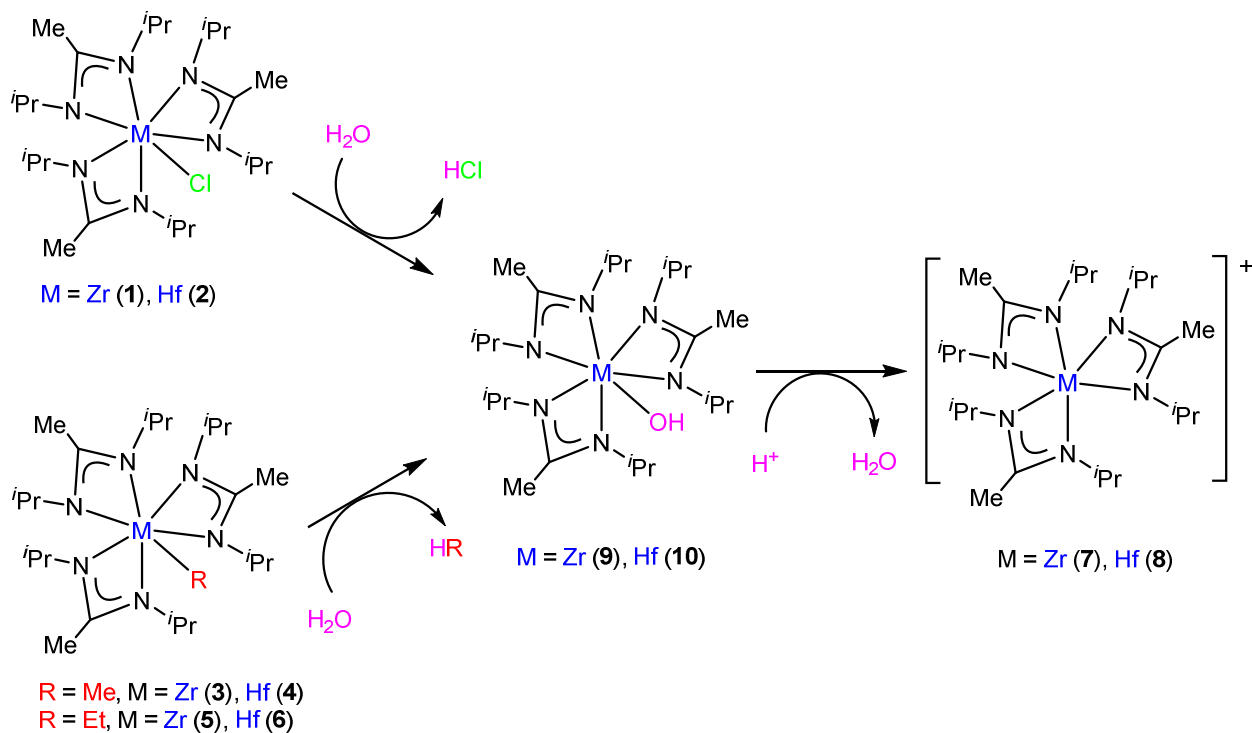
Fig. 4. Comparison of the ^1H NMR spectra of Zr-Cl (**1**), Zr-Me (**3**), and Zr-Et (**5**) in benzene- d_6 at 23 $^\circ\text{C}$.

MS studies of the reactions between 1-6 and H₂O in air

The process of loading and ionizing the air-sensitive samples using DART-MS may cause side reactions. Therefore, DART-MS provides an opportunity to study the reactions of the complexes with O₂ or H₂O and identify the products that may not be isolated.

DART-MS has been used to characterize and identify Zr-Cl (**1**) (Fig. S45) and Hf-Cl (**2**) (Fig. S48). However, **3-6** could not be identified directly in MS due to the presence of the labile alkyl groups. However, the hydroxyl complexes M[MeC(N^{*i*}Pr)₂]₃OH [M = Zr (**9**), Hf (**10**)] (Figs. S47 and S50) are identified as products in all MS spectra. These products stem from the reactions of the metal complexes with H₂O (Scheme 3) in air. These complexes undergo nucleophilic attack by water. This is followed by the release of HCl or HR (R = Me, Et) as well as forming Zr-OH (**9**) or Hf-OH (**10**). Since [Zr-OH (**9**)+H⁺] and [Hf-OH (**10**)+H⁺] are observed in the MS spectra, elimination of H₂O from the complexes would yield M[MeC(N^{*i*}Pr)₂]₃⁺ (**7-8**, Scheme 3, Figs. S46 and S49), which are also observed in the MS spectra.

Several attempts have been made to study the reactions of water with **1-6** on a larger scale in order to isolate Zr-OH (**9**), Hf-OH (**10**), M[MeC(N^{*i*}Pr)₂]₃⁺ (**7-8**), or other products. However, none was successful. These studies show that **1-6** are sensitive to water. When 1 equiv. of water is added to a solution of Zr-Et (**5**) in benzene-*d*₆, immediate reaction(s) occurs with the formation of insoluble white solids, ethane, and amidine ^{*i*}PrNH-C(Me)=N^{*i*}Pr. Ethane is identified in the ¹H NMR spectrum of the mixture. The presence of ^{*i*}PrNH-C(Me)=N^{*i*}Pr in the reaction mixture is confirmed by the ¹H and ¹³C NMR spectra and GC-MS analysis of the supernatant solution of the mixture.



Scheme 3. Reactions of Zr and Hf complexes **1-6** with water, yielding hydroxyl products Zr-OH (**9**), Hf-OH (**10**) and $M[\text{MeC}(\text{N}^i\text{Pr})_2]_3^+$ (**7-8**).

Conclusions

Six hepta-coordinate, Group 4 amidinate complexes have been prepared, isolated, and characterized. Crystal structures of Zr-Cl (**1**), Hf-Cl (**2**), Zr-Et (**5**), and Hf-Et (**6**) show that these complexes adopt a mono-capped octahedral geometry. Zr-Cl (**1**) and Hf-Cl (**2**) undergo exchanges between Δ and Λ enantiomers as studied via VT- ^1H NMR spectroscopy. The exchange rate of Hf-Cl (**2**) is larger than that of Zr-Cl (**1**). ^{15}N -HMBC technique has been used to obtain the ^{15}N signals for the amidinate ligands in **1-6**. The ^{15}N HMBC peaks and the α -C peaks in the $^{13}\text{C}\{^1\text{H}\}$ NMR are more upfield and downfield shifted, respectively, in the Hf complexes than in their Zr analogues.

Elevated temperatures are needed for Zr-Cl (**1**), Hf-Cl (**2**), Zr-Me (**5**), and Hf-Me (**6**) to obtain the ^{15}N HMBC signals. Thus, the exchanges of the enantiomers are more difficult in M-Cl (**1-2**) and M-Me (**3-4**) than in M-Et (**5-6**). The alkyl ligands in **3-6** appear to be more labile than the chloride ligands in **1-2**. They all undergo reactions with water in air, yielding hydroxyl products Zr-OH (**9**) and Hf-OH (**10**) in MS spectra.

Experimental section

All manipulations were carried out under a dry nitrogen atmosphere with the use of either a glovebox or standard Schlenk techniques. All glassware was flamed dried under vacuum. N,N'-Diisopropylcarbodiimide and MeLi (1.6 M in Et₂O) were purchased from Acros and used without further purification. ZrCl₄ and HfCl₄ (Strem) were sublimed at 170 °C and 0.01 torr before use. Li[MeC(NⁱPr)₂] was prepared by the reaction of N,N'-diisopropylcarbodiimide with MeLi by an approach similar to that of Hessen and coworkers.⁶⁹ EtCl was purchased from Eastman and diluted with benzene to 9.7 M before use. The solution was stored in a -32 °C freezer. Hexanes, pentane, benzene, THF, and EtO₂ were purified by distillation from potassium benzophenone ketyl. NMR solvents were dried and stored over 5 Å molecular sieves. ^1H , $^{13}\text{C}\{^1\text{H}\}$, $^1\text{H}-^{13}\text{C}$ HSQC, and VT ^1H NMR spectra for Zr-Cl (**1**) (Fig. 3) and Hf-Cl (**2**) (Fig. S41) were conducted on a Bruker Avance 400 MHz. VT ^1H NMR spectra for Zr-Cl (**1**) (Fig. S36) were also conducted on a Varian VNMRS-500 spectrometer. Activation parameters and rate constants were calculated using the VT ^1H spectra obtained from the Bruker Avance 400 MHz. Elemental analyses were conducted by Complete Analysis Laboratories, Inc., Parsippany, NJ. Mass spectra were recorded on a JEOL AccuTOF™ DART Mass

Spectrometer.

2-D ^1H - ^{15}N NMR experiments

2-D ^1H - ^{15}N -HMBC (Heteronuclear Multiple Bond Correlation) experiments, on unlabeled samples, were performed on a Varian (Agilent) 600 MHz liquid state NMR spectrometer, equipped with an inverse triple resonance probe. Parameters used for the ^{15}N -gHMBCAD are the following; number of scans, 4, number of increments, 200, delay between scans, 1 s, number of points 2884 and an acquisition time of 0.15 s. A filter of 8 Hz was used. Under these conditions, spectra were acquired in ~35 min. Processing and analysis of the spectra were done with MestreNova software.

The gHMBCAD pulse sequence is a magnitude mode 2-D HMBC experiment. It is a standard experiment on the VNMRJ package. The pulse sequence incorporates Pulsed Field Gradients (PFGs) and adiabatic (AD) radio frequency pulses. The advantage of PFGs is that almost a complete suppression of the parent signal is achieved, along with a dramatic reduction in the associated t_1 noise. The AD pulses, on the other hand, provide a much more uniform irradiation over the entire nitrogen spectral width helping in eliminating distortions of the signals.

Preparation of $\text{Zr}[\text{MeC}(\text{N}^i\text{Pr})_2]_3\text{Cl}$ (1)

Freshly sublimed ZrCl_4 (0.889 g, 0.00381 mol) was stirred in a 2:1 (v/v) hexanes/THF solution (30 mL) at $-40\text{ }^\circ\text{C}$ to form a slurry. The slurry was allowed to warm to room temperature and to stir overnight. The slurry was then cooled to $0\text{ }^\circ\text{C}$. $\text{Li}[\text{MeC}(\text{N}^i\text{Pr})_2]$ (1.715 g, 0.0116 mol) was dissolved in 2:1 (v/v) hexanes/THF (10 mL) and added dropwise to the ZrCl_4 slurry. The solution was allowed to warm to room temperature

over 2 h, and then heated at 35 °C for 16 h. Volatiles were removed in vacuo, and crude product was extracted with pentane (10-15 mL). The product was filtered, giving a bright yellow solution. The volume of the solution containing the crude product was reduced to ~5 mL. The solution was then put into a -32 °C freezer to afford light yellow crystals of **1** (1.280 g, 0.00233 mol, 61% yield based on ZrCl₄). ¹H NMR (benzene-*d*₆, 399.92 MHz, 23 °C): δ 3.53 (m, 6H, CHMe₂), 1.62 (s, 9H, NC(Me)N), 1.33 (br s, 36H, CHMe₂). ¹³C{¹H} NMR (benzene-*d*₆, 100.56 MHz, 23 °C): δ 174.7 (NC(Me)N), 48.3 (CHMe₂), 23.9 (CHMe₂), 12.8 (NC(Me)N). ¹H NMR (toluene-*d*₈, 399.92 MHz, 23 °C): δ 3.52 (m, 6H, CHMe₂), 1.64 (s, 9H, NC(Me)N), 1.31 (br s, 36H, CHMe₂); ¹³C{¹H} NMR (toluene-*d*₈, 100.56 MHz, 23 °C): δ 174.6 (NC(Me)N), 48.3 (CHMe₂), 23.9 (CHMe₂), 12.7 (NC(Me)N). ¹H NMR (toluene-*d*₈, 399.92 MHz, -80 °C) δ 3.52 (m, 3H, CHMe₂), 3.35 (m, 3H, CHMe₂), 1.64 (d, 9H, CHMe₂), 1.52 (s, 9H, NC(Me)N), 1.51 (d, 9H, CHMe₂), 1.16 (d, 9H, CHMe₂), 1.13 (d, 9H, CHMe₂), 1.34 (d, 9H, CHMe₂). ¹³C{¹H} NMR (toluene-*d*₈, 399.92 MHz, -80 °C): δ 174.5 (NC(Me)N), 48.2 (CHMe₂), 47.6 (CHMe₂), 23.7 (CHMe₂), 23.6 (CHMe₂), 12.8 (NC(Me)N). ¹⁵N NMR (benzene-*d*₆, 60.8 MHz, 60 °C): δ -183.23, -183.09 ppm. ¹H and ¹³C{¹H} NMR assignments were confirmed by ¹H-¹³C HSQC experiments. Anal. Calcd: C, 52.37; H, 9.34; N, 15.27. Found: C, 51.99; H, 9.13; N, 15.17. DART-MS: Calcd *m/z* = 549.2989 [**1**+H⁺], Found *m/z* = 549.33828 [**1**+H⁺].

Preparation of Hf[MeC(N^{*i*}Pr)₂]₃Cl (**2**)

A 2:1 (v/v) hexanes/THF solution (30 mL) was added to freshly sublimed HfCl₄ (1.201 g, 0.00375 mol) at -40 °C to form a slurry and allowed to stir overnight. The slurry was cooled to 0 °C. Li[MeC(N^{*i*}Pr)₂] (1.692 g, 0.0114 mol) was dissolved in a 2:1 (v/v)

hexanes/THF (10 mL). The Li[MeC(NⁱPr)₂] solution was added to the slurry dropwise. The solution was allowed to reach room temperature over 2 h, and then heated to 35 °C for 16 h. The volatiles were removed in vacuo, and the crude product extracted with pentane. The solution was filtered, and the volume reduced to ~5 mL. The solution flask was placed in a -32 °C freezer to give pale yellow crystals of **2** (1.153 g, 0.00181 mol, 48% yield based on HfCl₄). ¹H NMR (benzene-*d*₆, 399.92 MHz, 23 °C): δ 3.65 (m, 6H, CHMe₂), 1.62 (s, 9H, NC(Me)N), 1.33 (d, 36H, CHMe₂); ¹³C{¹H} NMR (benzene-*d*₆, 100.56 MHz, 23 °C): δ 174.1 (NC(Me)N), 48.0 (CHMe₂), 24.0 (CHMe₂), 13.3 (NC(Me)N). ¹H NMR (toluene-*d*₈, 399.92 MHz, 23 °C): δ 3.63 (m, 6H, CHMe₂), 1.64 (s, 9H, NC(Me)N), 1.29 (d, 36H, CHMe₂). ¹³C{¹H} NMR (toluene-*d*₈, 100.56 MHz, 23 °C): δ 174.0 (NC(Me)N), 48.0 (CHMe₂), 24.0 (CHMe₂), 13.2 (NC(Me)N). ¹H NMR (toluene-*d*₈, 399.92 MHz, -83 °C): δ 3.54 (br m, 3H, CHMe₂), 1.64 (d, 9H, CHMe₂), 1.51 (s, 9H, NC(Me)N), 1.51 (d, 9H, CHMe₂), 1.14 (d, 9H, CHMe₂), 1.12 (d, 9H, CHMe₂), 1.34 (d, 9H, CHMe₂). ¹³C{¹H} NMR (toluene-*d*₈, 399.92 MHz, -83 °C): δ 173.8 (NC(Me)N), 47.89 (CHMe₂), 47.2 (CHMe₂), 24.0 (CHMe₂), 23.5 (CHMe₂), 12.7 (NC(Me)N). ¹⁵N NMR (benzene-*d*₆, 60.8 MHz, 60 °C): δ -188.34, -188.31 ppm. ¹H and ¹³C{¹H} NMR assignments were confirmed by ¹H-¹³C HSQC experiments. Anal. Calcd: C, 45.21; H, 8.06; N, 13.18. Found: C, 45.11; H, 7.98; N, 12.97. DART-MS: DART-MS: Calcd *m/z* = 639.33987 [**2**+H⁺], Found *m/z* = 639.35548 [**2**+H⁺].

Synthesis of Zr[MeC(NⁱPr)₂]₃Me (**3**)

Zr[MeC(NⁱPr)₂]₃Me (**3**) was prepared by adding MeLi (0.70 mL, 1.6 M in Et₂O, 1.1 mmol) to Zr[MeC(NⁱPr)₂]₃Cl (**1**, 539.1 mg, 0.9795 mmol) at -40 °C in Et₂O. The solution was

allowed to stir for 16 h before volatiles were removed. Pentane was used to extract the crude product. After filtration, the volume of the solution was reduced. After cooling in a $-32\text{ }^{\circ}\text{C}$ freezer, white crystals of **3** formed (345.5 mg, 0.6519 mmol, 67% yield based on **1**). Though several attempts were made to use X-ray diffraction to study this compound, the crystals were not suitable for X-ray diffraction. ^1H NMR (benzene- d_6 , 399.84 MHz, $23\text{ }^{\circ}\text{C}$): δ 3.53 (m, 6H, CHMe_2), 1.68 (s, 9H, $\text{NC}(\text{Me})\text{N}$), 1.28 (d, 36H, CHMe_2), 0.81 (s, 3H, ZrMe). $^{13}\text{C}\{^1\text{H}\}$ NMR (benzene- d_6 , 100.54 MHz, $23\text{ }^{\circ}\text{C}$): δ 174.3 ($\text{NC}(\text{Me})\text{N}$), 49.4 (ZrMe , $J_{\text{C-H}} = 117\text{ Hz}$), 48.0 (CHMe_2), 24.5 (CHMe_2), 12.5 ($\text{NC}(\text{Me})\text{N}$). ^{15}N NMR (benzene- d_6 , 60.8 MHz, $45\text{ }^{\circ}\text{C}$): δ -188.78, -188.49. ^1H and $^{13}\text{C}\{^1\text{H}\}$ NMR assignments were confirmed by ^1H - ^{13}C HSQC and ^1H -gated-decoupled ^{13}C NMR experiments. Anal. Calcd: C, 56.66; H, 10.27; N, 15.86. Found: C, 56.50; H, 10.42; N, 15.77.

Synthesis of $\text{Hf}[\text{MeC}(\text{N}^i\text{Pr})_2]_3\text{Me}$ (**4**)

The synthesis of $\text{Hf}[\text{MeC}(\text{N}^i\text{Pr})_2]_3\text{Me}$ (**4**) was accomplished by adding $\text{Hf}[\text{MeC}(\text{N}^i\text{Pr})_2]_3\text{Cl}$ (**2**, 193.9 mg, 0.3041 mmol) to Et_2O and cooling the solution to $-40\text{ }^{\circ}\text{C}$. MeLi (0.20 mL, 1.6 M in Et_2O , 0.32 mmol) was added to the solution via syringe and stirred for 16 h. The volatiles are then removed. Pentane was added to the residue and the solution filtered to another flask. The solution containing crude product is reduced and put into a $-32\text{ }^{\circ}\text{C}$ freezer to afford clear crystals of **4** (94.1 mg, 0.1524 mmol, 50% yield based on **2**). The crystals were not suitable for X-ray diffraction. ^1H NMR (benzene- d_6 , 399.84 MHz, $23\text{ }^{\circ}\text{C}$): δ 3.64 (m, 6H, CHMe_2), 1.65 (s, 9H, $\text{NC}(\text{Me})\text{N}$), 1.27 (d, 36H, CHMe_2), 0.52 (s, 3H, HfMe). $^{13}\text{C}\{^1\text{H}\}$ NMR (benzene- d_6 , 100.54 MHz, $23\text{ }^{\circ}\text{C}$): δ 173.4 ($\text{NC}(\text{Me})\text{N}$), 54.7 (HfMe , $J_{\text{C-H}} = 111\text{ Hz}$), 47.8 (CHMe_2), 24.5 (CHMe_2), 13.1 ($\text{NC}(\text{Me})\text{N}$). ^{15}N NMR

(benzene- d_6 , 60.8 MHz, 45 °C): δ -191.97, -191.95. ^1H and $^{13}\text{C}\{^1\text{H}\}$ NMR assignments were confirmed by ^1H - ^{13}C HSQC and ^1H -gated-decoupled ^{13}C NMR experiments. Anal. Calcd: C, 48.65; H, 8.82; N, 13.62. Found: C, 48.48; H, 8.69; N, 13.83.

Synthesis of EtMgCl

The following procedure made it easier to handle EtCl. Separate solutions of benzene and EtCl were placed in ice baths. While still in the ice bath, benzene (45 g) was transferred to 100 g of EtCl. The solution was stored in the freezer until needed. EtMgCl was prepared using a modified procedure for synthesis of EtMgBr reagents.⁷⁰ A Schlenk flask was charged with Mg turnings (1.231 g, 0.05065 mol), and a single crystal of I_2 (~1 mg). Et_2O (~100 mL) was added and the solution was stirred at room temperature for 16 h. The Mg solution was then cooled to -50 °C. EtCl (4.5 mL EtCl in C_6H_6 , ~0.044 mol EtCl) was diluted in Et_2O (~10 mL) and also cooled to -50 °C. The EtCl was added to the Mg turnings dropwise. The reaction was slowly heated to 35 °C and allowed to stir overnight. The turbid solution was then allowed to cool to room temperature. The excess Mg turnings were removed via filtration. A small portion (~10 mL) of the solution was removed in vacuo to remove any unreacted EtCl. The concentration of EtMgCl (0.68 M) was determined via titration with a standard HCl solution. ^1H NMR (toluene- d_8 , 399.84 MHz, 23 °C): δ 1.62 (t, 3H, MgCH_2CH_3), -0.11 (m, 2H, MgCH_2CH_3). $^{13}\text{C}\{^1\text{H}\}$ NMR (toluene- d_8 , 100.54 MHz, 23 °C): δ 13.2 (MgCH_2CH_3), 2.0 (MgCH_2CH_3). The position of the CH_2 peak in the $^{13}\text{C}\{^1\text{H}\}$ NMR spectrum was confirmed by DEPT-135 NMR spectroscopy.

Synthesis of Zr[MeC(NⁱPr)₂]₃Et (**5**)

Zr[MeC(NⁱPr)₂]₃Cl (**1**, 346.8 mg, 0.6356 mmol) was dissolved in Et₂O and cooled to -30 °C. EtMgCl (1.0 mL, 0.68 M in Et₂O/C₆H₆, 0.68 mmol) was added via syringe. The solution was allowed to warm to room temperature over 3 h and stirred for 16 h.

Volatiles were removed in vacuo, and pentane was used to extract the crude product.

The solution was condensed and placed in a -32 °C freezer to afford yellow crystals of

Zr[MeC(NⁱPr)₂]₃Et (**5**, 161.0 mg, 0.2960 mmol, 47% yield based on **1**). ¹H NMR (benzene-*d*₆, 399.84 MHz, 23 °C): δ 3.66 (m, 6H, CHMe₂), 1.85 (t, 3H, ZrCH₂CH₃), 1.71 (s, 9H, NC(Me)N), 1.26 (d, 36H, CHMe₂), 1.06 (m, 2H, ZrCH₂CH₃). ¹³C{¹H} NMR (benzene-*d*₆, 100.54 MHz, 23 °C): δ 174.7 (NC(Me)N), 53.6 (ZrCH₂CH₃, J_{C-H} = 117 Hz), 47.6 (CHMe₂), 24.5 (CHMe₂), 16.1 (ZrCH₂CH₃), 14.0 (NC(Me)N). ¹H NMR (toluene-*d*₈, 399.84 MHz, 23 °C): δ 3.64 (m, 6H, CHMe₂), 1.74 (t, 3H, ZrCH₂CH₃), 1.73 (s, 9H, NC(Me)N), 1.24 (d, 36H, CHMe₂), 0.96 (m, 2H, ZrCH₂CH₃). ¹³C{¹H} NMR (toluene-*d*₈, 100.54 MHz, 23 °C): δ 174.7 (NC(Me)N), 53.8 (ZrCH₂CH₃), 47.7 (CHMe₂), 24.50 (CHMe₂), 16.1 (ZrCH₂CH₃), 14.0 (NC(Me)N). ¹⁵N NMR (benzene-*d*₆, 60.8 MHz, 25 °C): δ -187.95, -187.87. ¹H and ¹³C{¹H} NMR assignments were confirmed by ¹H-¹³C HSQC, DEPT-135, and ¹H-gated-decoupled ¹³C NMR experiments. Anal. Calcd: C, 57.40; H, 10.38; N, 15.45. Found: C, 57.24; H, 10.19; N, 15.28.

Synthesis of Hf[MeC(NⁱPr)₂]₃Et (**6**)

EtMgCl (0.80 mL, 0.6796 M in Et₂O/C₆H₆, 0.54 mmol) was added via syringe to a solution of Hf[MeC(NⁱPr)₂]₃Cl (**2**, 333.1 mg, 0.5224 mmol) in Et₂O at -30 °C. The solution

was allowed to warm to room temperature and stir overnight. Volatiles were removed in vacuo. Pentane was used to extract the crude product. After filtration, the volume of the solution was reduced, and the flask was placed in a -32 °C freezer to afford pale yellow crystals of Hf[MeC(NⁱPr)₂]₃Et (**6**, 196.5 mg, 0.3113 mmol, 59% yield based on **2**). ¹H NMR (benzene-*d*₆, 399.84 MHz, 23 °C): δ 3.74 (m, 6H, CHMe₂), 2.01 (t, 3H, HfCH₂CH₃), 1.69 (s, 9H, NC(Me)N), 1.25 (d, 36H, CHMe₂), 0.73 (m, 2H, HfCH₂CH₃). ¹³C{¹H} NMR (benzene-*d*₆, 100.54 MHz, 23 °C) δ 173.9 (NC(Me)N), 58.2 (HfCH₂CH₃, *J*_{C-H} = 117 Hz), 47.4 (CHMe₂), 24.5 (CHMe₂), 16.3 (HfCH₂CH₃), 14.6 (NC(Me)N). ¹H NMR (toluene-*d*₈, 399.84 MHz, 23 °C): δ 3.72 (m, 6H, CHMe₂), 1.91 (t, 3H, HfCH₂CH₃), 1.70 (s, 9H, NC(Me)N), 1.23 (d, 36H, CHMe₂), 0.64 (m, 2H, HfCH₂CH₃). ¹³C{¹H} NMR (toluene-*d*₈, 100.54 MHz, 23 °C): δ 173.8 (NC(Me)N), 58.2 (HfCH₂CH₃), 47.4 (CHMe₂), 24.5 (CHMe₂), 16.3 (HfCH₂CH₃), 14.5 (NC(Me)N). ¹⁵N NMR (benzene-*d*₆, 60.8 MHz, 25 °C): δ -191.29, -191.20. ¹H and ¹³C{¹H} NMR assignments were confirmed by ¹H-¹³C HSQC, DEPT-135, and ¹H-gated-decoupled ¹³C NMR experiments. Anal. Calcd: C, 49.47; H, 8.94; N, 13.31. Found: C, 49.00; H, 8.60; N, 15.28.

Calculating errors in VT NMR studies

The activation parameters for Zr-Cl (**1**) and Hf-Cl (**2**) determined from their Eyring plots were obtained by using the average rate constants which were obtained through two separate experiments at a given temperature. The averages are listed in Tables S7 and S8. The maximum random uncertainty in the rate constants was combined with the estimated systematic uncertainty of 5%. The total uncertainties in the rate constants *k* were used in the ln(*k*_{eq}/*T*) vs. 1000/*T* plot in Figs S37-S40 for Zr-Cl (**1**) and Figs. S42-

S44 for Hf-Cl (**2**), and error calculations. Temperature measurements of the NMR probe contribute to an estimated uncertainty of 1 K. The uncertainties in ΔH^\ddagger and ΔS^\ddagger were calculated from the following error formulas (Eqs. 2-3) derived from $R \ln(kh/k_b T) = -\Delta H^\ddagger/T + \Delta S^\ddagger$.⁷¹

$$(\sigma\Delta H^\ddagger)^2 = \frac{R^2 T_{\max}^2 T_{\min}^2}{\Delta T^2} \left\{ \left(\frac{\sigma T}{T} \right)^2 \left[\left(1 + T_{\min} \frac{\Delta L}{\Delta T} \right)^2 + \left(1 + T_{\max} \frac{\Delta L}{\Delta T} \right)^2 \right] + 2 \left(\frac{\sigma k}{k} \right)^2 \right\} \quad (\text{Eq. 2})$$

2)

$$(\sigma\Delta S^\ddagger)^2 = \frac{R^2}{\Delta T^2} \left\{ \left(\frac{\sigma T}{T} \right)^2 \left[T_{\max}^2 \left(1 + T_{\min} \frac{\Delta L}{\Delta T} \right)^2 + T_{\min}^2 \left(1 + T_{\max} \frac{\Delta L}{\Delta T} \right)^2 \right] + \left(\frac{\sigma k}{k} \right)^2 (T_{\max}^2 + T_{\min}^2) \right\} \quad (\text{Eq. 3})$$

3)

where $\Delta L = [\ln(k_{\max}/T_{\max}) - \ln(k_{\min}/T_{\min})]$ and $\Delta T = (T_{\max} - T_{\min})$.

Determination of the X-ray crystal structures of **1**, **2**, **5** and **6**

The X-ray structures of Zr-Cl (**1**), Hf-Cl (**2**), Zr-Et (**5**) and Hf-Et (**6**) were determined on a Bruker ASX Smart 1000 X-ray diffractometer equipped with a CCD area detector and a graphite-monochromated Mo source ($K\alpha$ radiation, 0.71073 Å) and fitted with an upgraded Nicolet LT-2 low temperature device. A suitable crystal was chosen from a batch and was coated paratone oil (Exxon). The crystal was mounted onto the diffractometer using a fiber loop under a stream of nitrogen at 100(2) K. The structure was solved by direct methods, and all non-hydrogen atoms were refined anisotropically using Olex2 software. Since the crystals for both Zr-Cl (**1**) and Hf-Cl (**2**) were twinned, TWINABS was used for the absorption corrections. The twin laws (TWIN -1 0 -0.071 0 -

1 0 0 0 1, and BASF 0.0839) and (TWIN -1 0 0 0 -1 0 0.175 0 1, and BASF 0.3297) were used for Zr-Cl (**1**) and Hf-Cl (**2**), respectively. Global refinements for the unit cells and data reduction were performed using the Saint program (Version 6.02). Calculations of atom positions were done using SHELXTL (Version 5.1) proprietary software package and Olex2.⁷²⁻⁷⁵

Mass spectrometric studies of 1-6

Mass spectra were recorded on a JEOL AccuTOF™ DART Mass Spectrometer. The closed end of a capillary tube was inserted into either solid powders or a solution (in pentane) of the samples. The tube was then placed into a heated stream of He (200 °C) in the spectrometer. The spectra were referenced to a polyethylene glycol (PEG) standard.

Electronic supplementary information (ESI) available: ORTEPs of **1** and **5**, crystallographic refinement data, selected bond lengths and angles, 1-D and 2-D NMR spectra, VT-NMR spectra of **1** and **2**, rate constants, Eyring plots, and DART-MS spectra. CCDC Nos. for **1-2** and **5-6** are: 1850476 (**1**), 1850478 (**2**), 1850477 (**5**) and 1850480 (**6**).

Conflicts of interest

There are no conflicts to declare.

Acknowledgements

The authors thank the US National Science Foundation (CHE-1633870) for supporting

the research, Prof. Michael G. Richmond and Dr. David A. Hrovat for helpful discussions, and Dr. Patrick Hillesheim for assistance in refining the crystal structures.

References

1. C. Stanciu, M. E. Jones, P. E. Fanwick and M. M. Abu-Omar, *J. Am. Chem. Soc.*, 2007, **129**, 12400-12401.
2. T. D. Tilley, *Organometallics*, 1985, **4**, 1452-1457.
3. T. F. Blackburn, J. A. Labinger and J. Schwartz, *Tetrahedron Lett.*, 1975, **16**, 3041-3044.
4. T. V. Lubben and P. T. Wolczanski, *J. Am. Chem. Soc.*, 1987, **109**, 424-435.
5. R. Wang, K. Folting, J. C. Huffman, L. R. Chamberlain and I. P. Rothwell, *Inorg. Chim. Acta*, 1986, **120**, 81-83.
6. V. C. Gibson, C. Redshaw, G. P. Walker, J. K. Howard, V. Hoy, J. M. Cole, L. G. Kuzmina and D. S. De Silva, *J. Chem. Soc., Dalton Trans.*, 1999, **0**, 161-166.
7. C. J. Schaverien and A. G. Orpen, *Inorg. Chem.*, 1991, **30**, 4968-4978.
8. X. Liu and D. Cui, *Dalton Trans.*, 2008, 3747-3752.
9. A. Van Asselt, M. S. Trimmer, L. M. Henling and J. E. Bercaw, *J. Am. Chem. Soc.*, 1988, **110**, 8254-8255.
10. P. B. Brindley and J. C. Hodgson, *J. Organomet. Chem.*, 1974, **65**, 57-64.
11. B. J. Boro, R. Lansing, K. I. Goldberg and R. A. Kemp, *Inorg. Chem. Commun.*, 2011, **14**, 531-533.
12. F. Lu, R. A. Zarkesh and A. F. Heyduk, *Eur. J. Inorg. Chem.*, 2012, **2012**, 467-470.
13. M. H. Chisholm, C. E. Hammond and J. C. Huffman, *J. Chem. Soc., Chem.*

- Commun.*, 1987, 1423-1424.
14. R. Wang, X.-H. Zhang, S.-J. Chen, X. Yu, C.-S. Wang, D. B. Beach, Y.-D. Wu and Z.-L. Xue, *J. Am. Chem. Soc.*, 2005, **127**, 5204-5211.
 15. S.-J. Chen, X.-H. Zhang, X. Yu, H. Qiu, G. P. A. Yap, I. A. Guzei, Z. Lin, Y.-D. Wu and Z.-L. Xue, *J. Am. Chem. Soc.*, 2007, **129**, 14408-14421.
 16. S.-J. Chen, J. Zhang, X. Yu, X. Bu, X.-T. Chen and Z.-L. Xue, *Inorg. Chem.*, 2010, **49**, 4017-4022.
 17. L. A. Morton, M. Miao, T. M. Callaway, T. Chen, S.-J. Chen, A. A. Tuinman, X. Yu, Z. Lu and Z.-L. Xue, *Chem. Commun.*, 2013, **49**, 9555-9557.
 18. T. Chen, X.-H. Zhang, C. Wang, S. Chen, Z. Wu, L. Li, K. R. Sorasaene, J. B. Diminnie, H. Pan, I. A. Guzei, A. L. Rheingold, Y.-D. Wu and Z.-L. Xue, *Organometallics*, 2005, **24**, 1214-1224.
 19. H. Qiu, S.-J. Chen, C.-S. Wang, Y.-D. Wu, I. A. Guzei, X.-T. Chen and Z.-L. Xue, *Inorg. Chem.*, 2009, **48**, 3073-3079.
 20. X. Yu, X.-T. Chen and Z.-L. Xue, *Organometallics*, 2009, **28**, 6642-6645.
 21. S. Chen, G. P. A. Yap and Z. Xue, *Sci. China, Ser. B: Chem.*, 2009, **52**, 1583-1589.
 22. S. Chen, X. Zhang, Z. Lin, Y. Wu and Z. Xue, *Sci. China, Ser. B: Chem.*, 2009, **52**, 1723-1733.
 23. S.-J. Chen and Z.-L. Xue, *Organometallics*, 2010, **29**, 5579-5584.
 24. B. Sharma, T. M. Callaway, A. C. Lamb, C. A. Steren, S.-J. Chen and Z.-L. Xue, *Inorg. Chem.*, 2013, **52**, 11409-11421.
 25. J. Hong, L. Zhang, K. Wang, Z. Chen, L. Wu and X. Zhou, *Organometallics*,

- 2013, **32**, 7312-7322.
26. T. M. Cook, A. C. Lamb and Z.-L. Xue, *Chinese J. Inorg. Chem*, 2017, **33**, 1947-1958.
 27. F. T. Edelman, *Chem. Soc. Rev.*, 2012, **41**, 7657-7672.
 28. S. T. Barry, *Coord. Chem. Rev.*, 2013, **257**, 3192-3201.
 29. K. H. Theopold, O. M. Reinaud, S. Blanchard, S. Leelasubcharoen, A. Hess and S. Thyagarajan, in *Advancing Sustainability through Green Chemistry and Engineering*, ACS Symp. Series, 2002, vol. 823, Ch. 6, pp. 75-85.
 30. A. N. Campbell and S. S. Stahl, *Acc. Chem. Res.*, 2012, **45**, 851-863.
 31. R. A. Himes and K. D. Karlin, *Curr. Opin. Chem. Biol.*, 2009, **13**, 119-131.
 32. A. C. Lamb, Z. Lu and Z.-L. Xue, *Chem. Commun.*, 2014, **50**, 10517-10520.
 33. A. C. Lamb, Z. Wang, T. M. Cook, B. Sharma, S.-J. Chen, Z. Lu, C. A. Steren, Z. Lin and Z.-L. Xue, *Polyhedron*, 2016, **103**, 2-14.
 34. I. M. Klotz and D. M. Kurtz, *Chem. Rev.*, 1994, **94**, 567-568.
 35. V. Krisyuk, L. Aloui, N. Prud'homme, S. Sysoev, F. Senocq, D. Samélor and C. Vahlas, *Electrochem. Solid-State Lett.*, 2011, **14**, D26-D29.
 36. T. B. Thiede, M. Krasnopolski, A. P. Milanov, T. de los Arcos, A. Ney, H.-W. Becker, D. Rogalla, J. Winter, A. Devi and R. A. Fischer, *Chem. Mater.*, 2011, **23**, 1430-1440.
 37. M. Eleter, L. G. Hubert-Pfalzgraf, S. Daniele, G. Pilet and B. Tinant, *Polyhedron*, 2010, **29**, 2522-2526.
 38. V. R. Pallem; C. Dussarrat; American Air Liquide, Inc.; Vol. WO 2012138332.
 39. K. Takahashi, H. Funakubo, S. Hino, M. Nakayama, N. Ohashi, T. Kiguchi and E.

- Tokumitsu, *J. Mater. Res.*, 2011, **19**, 584-589.
40. H. T. Chiu, C. N. Wang and S. H. Chuang, *Chem. Vap. Deposition*, 2000, **6**, 223-225.
41. J. S. M. Lehn, S. Javed and D. M. Hoffman, *Chem. Vap. Deposition*, 2006, **12**, 280-284.
42. T. Elkin and M. S. Eisen, *Catal. Sci. Technol.*, 2015, **5**, 82-95.
43. X. Yu, Q. You, X. Zhou and L. Zhang, *ACS Catalysis*, 2018, **8**, 4465-4472.
44. K. Weitershaus, B. D. Ward, R. Kubiak, C. Muller, H. Wadepohl, S. Doye and L. H. Gade, *Dalton Trans.*, 2009, 4586-4602.
45. J.-F. Sun, S.-J. Chen, Y. Duan, Y.-Z. Li, X.-T. Chen and Z.-L. Xue, *Organometallics*, 2009, **28**, 3088-3092.
46. S. Ren, Z. Qiu and Z. Xie, *Organometallics*, 2013, **32**, 4292-4300.
47. D. Casanova, P. Alemany, J. M. Bofill, S. Alvarez, D. Casanova, P. Alemany, J. M. Bofill and S. Alvarez, *Chem.-Eur. J.*, 2003, **9**, 1281-1295.
48. R. Hoffmann, B. F. Beier, E. L. Muetterties and A. R. Rossi, *Inorg. Chem.*, 1977, **16**, 511-522.
49. D. L. Kepert, *Prog. Inorg. Chem.*, 2007, **25**, 41-144.
50. Z. Lin and I. Bytheway, *Inorg. Chem.*, 1996, **35**, 594-603.
51. M. G. B. Drew, *Prog. Inorg. Chem.*, 1997, **23**, 67-210.
52. R. M. Haas, M. Arshad, J. Anthony, P. J. Altmann, A. Pothig, F. H. Kohler and C. R. Hess, *Inorg. Chem. Front.*, 2016, **3**, 616-629.
53. A. Zalkin, D. H. Templeton and D. G. Karraker, *Inorg. Chem.*, 1969, **8**, 2680-2684.

54. L. Yan, X. Wang and M. Zhou, *Inorg. Chem. Commun.*, 2016, **65**, 32-34.
55. R. C. Bray, B. Adams, A. T. Smith, B. Bennett and S. Bailey, *Biochemistry*, 2000, **39**, 11258-11269.
56. S. T. Rao, K. A. Satyshur, M. L. Greaser and M. Sundaralingam, *Acta Crystallogr., Sect. D: Biol. Crystallogr.*, 1996, **52**, 916-922.
57. A. S. McAlpine, A. G. McEwan, A. L. Shaw and S. Bailey, *JBIC, J. Biol. Inorg. Chem.*, 1997, **2**, 690-701.
58. M. Zhou, H. Tong, X. Wei and D. Liu, *J. Organomet. Chem.*, 2007, **692**, 5195-5202.
59. M. Galajov, C. Garcia, M. Gomez and P. Gomez-Sal, *Dalton Trans.*, 2014, **43**, 5747-5758.
60. M. Galajov, C. Garcia and M. Gomez, *Dalton Trans.*, 2011, **40**, 413-420.
61. M. Galajov, C. Garcia, M. Gomez and P. Gomez-Sal, *Dalton Trans.*, 2011, **40**, 2797-2804.
62. K. Xu, A. P. Milanov, M. Winter, D. Barreca, A. Gasparotto, H.-W. Becker and A. Devi, *Eur. J. Inorg. Chem.*, 2010, **2010**, 1679-01688.
63. J.-F. Sun, X.-T. Chen and Z.-L. Xue, *Inorg. Chim. Acta*, 2009, **362**, 4251-4254.
64. Z.-L. Xue, T. M. Cook and A. C. Lamb, *J. Organomet. Chem.*, 2017, **852**, 74-93.
65. J. C. Bailar, *J. Inorg. Nucl. Chem.*, 1958, **8**, 165-175.
66. J. Sandstrom, *Dynamic NMR Spectroscopy*, Academic Press, 1982.
67. R. S. Macomber, *A Complete Introduction to Modern NMR Spectroscopy*, Wiley, 1998.
68. The rate constants here are the chemical rate constants, and they differ from the

- observed magnetization transfer rate constants by a factor of 2.
69. S. Ge, A. Meetsma and B. Hessen, *Organometallics*, 2008, **27**, 3131.
 70. A. Glockner, H. Bauer, M. Maekawa, T. Bannenberg, C. G. Daniliuc, P. G. Jones, Y. Sun, H. Sitzmann, M. Tamm and M. D. Walter, *Dalton Trans.*, 2012, **41**, 6614-6624.
 71. P. M. Morse, M. D. Spencer, S. R. Wilson and G. S. Girolami, *Organometallics*, 1994, **13**, 1646-1655.
 72. G. M. Sheldrick. In *SHELXL-2018, A Program for the Refinement of Crystal Structures* University of Göttingen, Göttingen, Germany, 2018.
 73. G. M. Sheldrick, SADABS: Software for Empirical Absorption Correction, version 2.05, University of Göttingen, Göttingen, Germany, 2002.
 74. G. M. Sheldrick, TWINABS: Software for Empirical Absorption Correction, version 2.05, University of Göttingen, Göttingen, Germany, 2002.
 75. O. V. Dolomanov, L. J. Bourhis, R. J. Gildea, J. A. K. Howard and H. Puschmann, *J. Appl. Crystallogr.*, 2009, **42**, 339-341.

Graphical abstract

Hepta-coordinated Group 4 amidinate complexes have been synthesized and characterized including by ^{15}N chemical shifts through ^1H - ^{15}N gHMBC NMR.

